DOI: 10.1002/adem.200800283

Dislocations as Active Components in Novel Silicon Devices**

By *Martin Kittler** and *Manfred Reiche**

The electrical and optical properties of dislocations in Si are reviewed, namely dislocation-related recombination and luminescence, transport of minority and majority carriers along dislocations or the electric field around dislocations. It is shown that Si wafer direct bonding allows well-controlled formation of dislocation networks, giving rise to adjustable dislocation properties. Ideas for novel Si devices utilizing dislocations as active components are presented. In particular, dislocation-based light emitters at about 1.5 µm wavelength are demonstrated. Concepts for dislocation-based conductive channels and fast FETs, manipulators of biomolecules or thermo-electric generators are sketched.

1. Introduction

Dislocations are extended, quasi one-dimensional imperfections in crystalline solids or in other words "native nanowires" embedded in the crystal lattice that exhibit unique properties. With the exception of internal gettering in Si, semiconductor technology traditionally intends to avoid the formation of crystal defects like dislocations because of their detrimental effects on device performance. On the other hand, there have been attempts to utilize dislocations as active components in semiconductor devices for already 40–50 years. Starting from suggestions in the 1970s to apply the "self-organized" diode behavior of dislocations in Ge[1] and Si[2,3] and in the 1980s to use dislocations as buried microwires in Si[4] to the recently proposed application of dislocations as a base for Si light emitters, dislocations were always in the center of the attention of semiconductor specialists.

The lack of an appropriate technology for well-controlled fabrication of dislocations regarding their structure, electrical and optical properties, location, state of decoration with impurities, etc., was the main obstacle for exploiting their unique properties. However, Si wafer direct bonding allows the formation of regular periodic dislocation networks in a reproducible manner.

In this paper, we will sketch in chapter 2 important electrical and optical properties of dislocations in Si. In chapter 3 dislocation networks will be introduced that can be produced by silicon wafer direct bonding. Then potential application of such dislocation networks for novel Si devices will be addressed in chapter 4. In detail, we will discuss the use of dislocations in Si-based light emitters. Moreover, we will shortly sketch possible application of extremely enhanced transport of charge carriers along dislocations and other applications, e.g., for Si-based thermo-electrical generators or for spatial control of biomolecule immobilization on Si surfaces.

2. Properties of Dislocations in Si

2.1. About Dislocations in Si

Dislocations represent line defects in the regular crystal lattice of solids and may be regarded as a kind of a "native nanowires". According to a simple geometric picture, dislocations in the diamond structure of the Si lattice are connected with dangling (broken) bonds, e.g.,[5] see Figure 1. There exist also many other defects and lattice irregularities in the dislocation core and at/around the dislocations of either intrinsic origin, i.e., kinks, jogs, etc., or of extrinsic origin, i.e.,

[*] *Prof. M. Kittler*
IHP, Im Technologiepark 25
15236 Frankfurt (Oder), Germany
IHP/BTU Joint Lab, Konrad-Wachsmann-Allee 1
03046 Cottbus, Germany
E-mail: kittler@ihp-microelectronics.com
Dr. M. Reiche
MPI für Mikrostrukturphysik, Weinberg 2
06120 Halle, Germany
E-mail: reiche@mpi-halle.mpg.de

[**] *Acknowledgments, Parts of this work were done within the framework of the SILEM project, funded by the BMBF Ministry, and of the SOBSI project, funded by the Volkswagenstiftung Hannover. We would like to thank T. Mchedlidze, T. Arguirov, W. Seifert, O. Vyvenko, T. Wilhelm, and X. Yu for supporting this work.*

 © 2009 WILEY-VCH Verlag GmbH & Co. KGaA, Weinheim

REVIEW

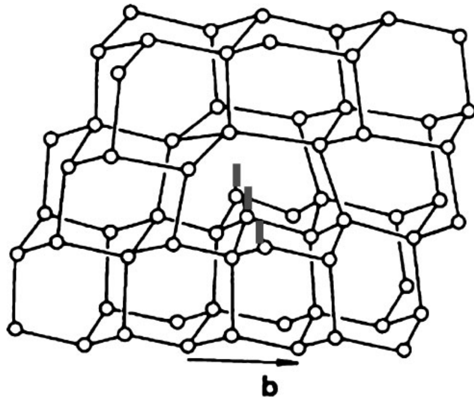

Fig. 1. 60° dislocation with dangling bonds in the diamond lattice, after Hornstra.[5]

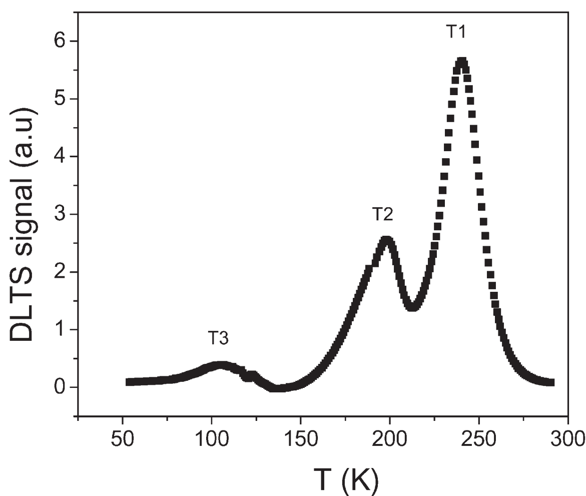

Fig. 2. DLTS spectrum of a dislocation network in p-type Si, showing levels located at approximately 0.08, 0.3, and 0.4 eV above the valence band, respectively.

impurity atoms; for more details see, e.g., ref.[6] They all are known to cause states in the forbidden gap of Si between the valence and conduction band. As an example, Figure 2 displays a DLTS spectrum exhibiting three dislocation-related levels of a dislocation network in p-type Si.

Dislocation-related states can be occupied with electrons in n-type Si forming a negative line charge Γ. To keep space charge neutrality the negatively charged dislocation line in n-Si is surrounded with a cylinder of ionized (positively charged) donor atoms, the so-called Read cylinder. In the opposite case of p-type Si the dislocations form positively charged lines surrounded with ionized (negatively charged) acceptor atoms. A consequence of the structure formed by a charged dislocation line being surrounded with a Read cylinder is the bending of the conduction and valence bands, i.e., the appearance of a barrier in the band scheme which is associated with the occurrence of an electric field. This is schematically demonstrated in Figure 3. The radius of the Read cylinder is given by $R = (\Gamma/\pi\ qN_{\mathrm{dot}})^{1/2}$, where N_{dot} is the dopant concentration. The barrier can be approximately described[7] by $\Phi = \Gamma/(2\pi\ \varepsilon_{\mathrm{Si}}) \times \ln(\Gamma\ \lambda_{\mathrm{D}}/q)$ with $\varepsilon_{\mathrm{Si}}$ the dielectric constant of Si, λ_{D} the Debye screening length and q the elementary charge.

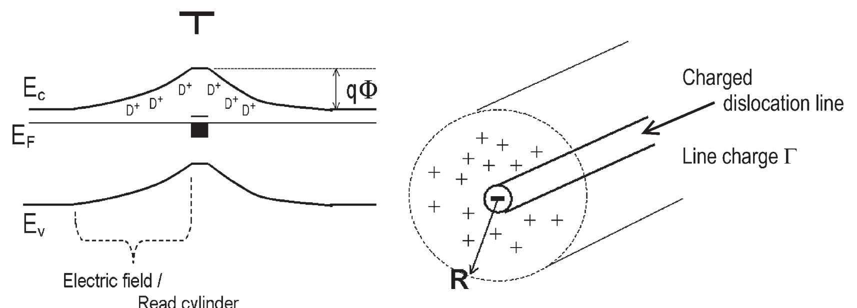

Fig. 3. Band scheme of a charged dislocation line and Read cylinder for n-type Si.

The dislocation line charge Γ has major influence on the barrier and, hence, on the electric field around the dislocations. Typically, the average electric field $E = \Phi/R$ may reach values around $10^4\ \mathrm{V\,cm^{-1}}$.

2.2. Influence of Metals and Hydrogen on Electrical and Optical Properties of Dislocations in Si

In general, the dislocation properties strongly depend on the thermal history of dislocations and on the impurity content in the Si material, since these factors determine the density of intrinsic defects in the dislocation core as well as of impurities decorating the dislocation. Figure 4 illustrates clearly that the recombination activity of dislocations may differ strongly owing to the degree of dislocation contamination.

''Clean'' dislocations exhibit only very small electrical activity.[8,9] Accommodation of even tiny amounts of metal atoms at the dislocations may have pronounced impact on dislocation activity. Predominantly metal and oxygen atoms at the dislocations have been reported to substantially influence the optical and electrical properties, e.g., ref.[8,10,11] In contrast, hydrogen is mostly found to passivate the impact of foreign atoms, see, e.g., ref.[12] regarding dislocation luminescence and[13] regarding defect recombination activity.

2.2.1. Influence of Metal Contamination on c(T) Behavior

The temperature dependence of the dislocation recombination activity expressed by the electron-beam-induced-current (EBIC) contrast, c(T), depends on the contamination with metals.[8] According to the model of recombination described in,[14] the line density N_{M} of deep states caused by impurities at the dislocations determines the recombination activity and its temperature dependence. The interaction of carriers in the strain-induced one-dimensional dislocation bands with deep impurities at/near the dislocation is essential for a proper description of the recombination activity.[14] Simulations of the c(T) dependence for different line densities of deep states at the dislocation (Fig. 5) are in good agreement

 © 2009 WILEY-VCH Verlag GmbH & Co. KGaA, Weinheim

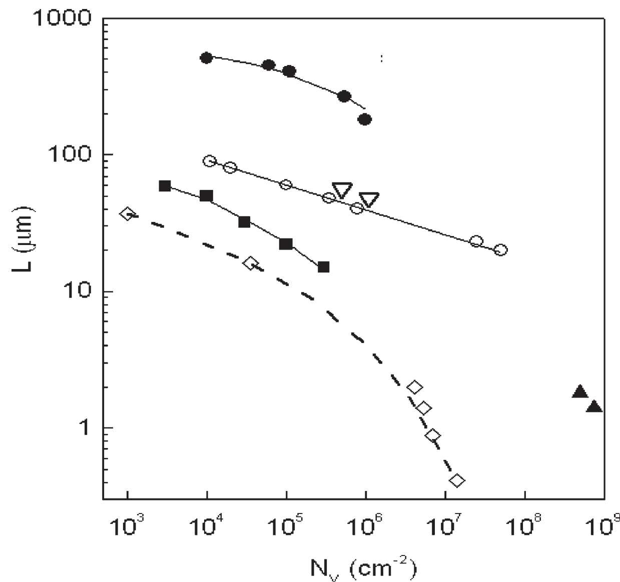

Fig. 4. Minority-carrier diffusion length L versus dislocation density N_V in different Si materials. The recombination activity of the dislocations, which manifests itself in the decrease in L with increasing N_V, differs largely between the materials due to the different degree of contamination.

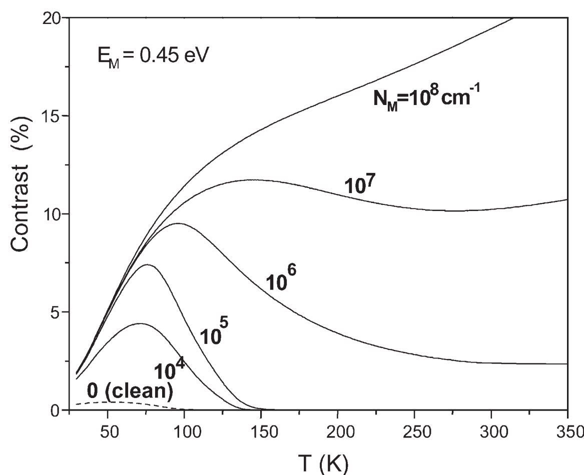

Fig. 5. Simulated temperature dependence c(T) of the recombination activity of dislocations, parameter: line density of deep states N_M, see also.[14]

with experimental observations. It is seen from the simulation data that even a very small metal contamination of only $N_M = 10^4\,cm^{-1} = 1\,\mu m^{-1}$ causes a remarkable effect on recombination, although only at low temperatures. Up to concentrations N_M of a few $10^5\,cm^{-1}$ the room temperature (RT) activity remains low and the activity increases with decreasing temperatures. The temperature dependence changes its character at high line densities of impurities, with the largest activity observed at RT. It is worth to note, that the c(T) behavior allows a sensitive estimation of the level of impurities accommodated at dislocations.

The line density of deep states at dislocations may cause to substantial barriers. Although we have $\Gamma < qN_M$ for the dislocation line charge due to incomplete occupation of states, dislocation barriers larger than 100 mV can be achieved,[15] in particular for heavily contaminated dislocations.

Grain boundaries (GBs) can be regarded as planar arrangement of dislocations. The above considerations for dislocations are therefore qualitatively valid for GBs too. As dislocations, GBs may show potential barriers, with height depending on the type of the boundary and its contamination with impurities. Such barriers at GBs can be detected with the so-called GB-EBIC technique, which utilizes the electrical field of the GB barrier to separate beam induced charge carriers. Figure 6 presents an example of a GB in Si. The black/white contrast is due to the reversal of the direction of the electric field when crossing the boundary.

2.2.2. Hydrogen Passivation

Hydrogen passivation is a standard means to improve the recombination properties of solar Si materials. EBIC studies on dislocations and GBs have shown that the recombination activity at RT and, accordingly, the density of impurity levels at dislocations and GBs can be significantly reduced by a hydrogenation treatment, e.g., ref.[13,16] However, it has been observed that hydrogen cannot completely remove all the impurity-induced deep states at defects. Besides its impact on recombination, hydrogenation has also been found to reduce the barrier height at GBs.

2.3. Transport of Charge Carriers by Dislocations in Si

One-dimensional conductive channels formed by defects in solar Si have already been demonstrated (for details see, e.g.,[17]). An analysis of dislocation networks in Si revealed a similar feature. The EBIC micrograph in Figure 7 shows a vertical bright line extending from the Schottky contact on the upper left corner, vertically over a large distance. This demonstrates transport of minority carriers along the dislocation network toward the collecting Schottky barrier. The transport of minority carriers over distances > 10 mm has been observed by EBIC and LBIC.[17a,18] In another experiment, we

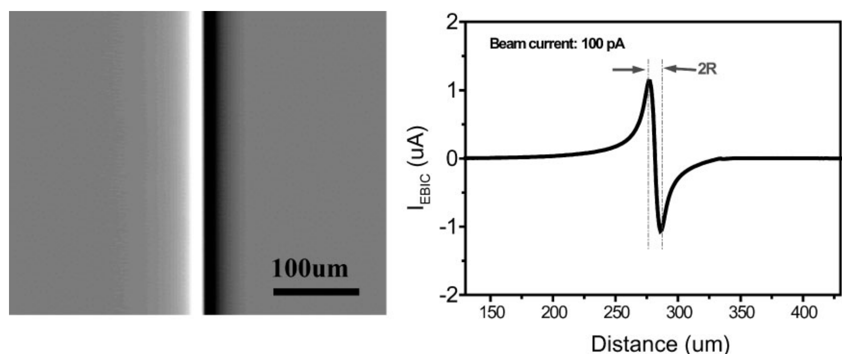

Fig. 6. Evidence of potential barrier at a GB in p-type Si from GB-EBIC investigations.[15] a) GB-EBIC image, b) current profile at the boundary.

© 2009 WILEY-VCH Verlag GmbH & Co. KGaA, Weinheim

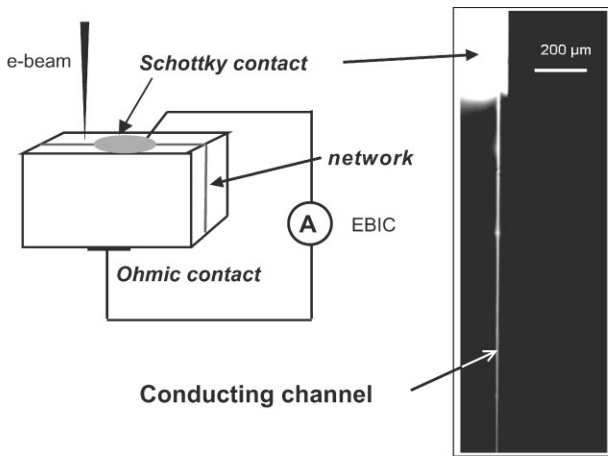

Fig. 7. Conducting channel at a bonded dislocation network: sketch of experimental setup (left) and EBIC micrograph revealing a conducting channel (right).

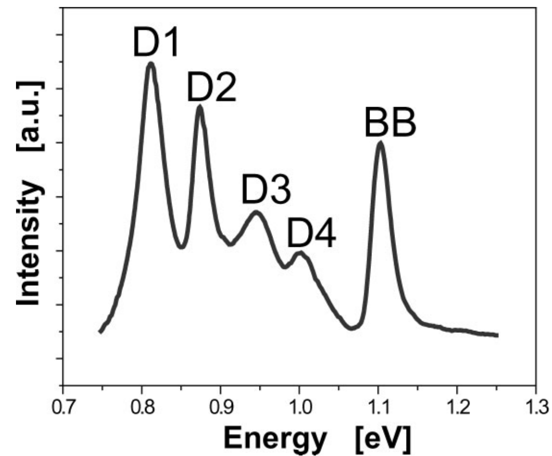

Fig. 9. Dislocation D line luminescence: Spectrum of dislocated silicon, showing D1–D4 dislocation lines and band–band line.

observed a strong influence of dislocations on the resistance which is related to majority carriers[17b]. A dislocation network was formed within a 40 nm thick Silicon-on-Insulator (SOI) layer with p-type conductivity and Ohmic contacts were fabricated at a distance of 1 µm, see Figure 8a. The *I–V* characteristics measured at 300 K is shown in Figure 8b and exhibits Ohmic character. The resistance of the structure yielded about $R_{\mathrm{disl}} = 4 \times 10^{2}\,\Omega$. For the similar reference structure, without a dislocation network in the 40 nm thick SOI layer, a resistance of $R_{\mathrm{ref}} = 2 \times 10^{6}\,\Omega$ was found. Recently, Ishikawa reported a reduction of *R* caused by a dislocation network in a p-type SOI layer.[19] According to his suggestion the dislocations form ''n-channels'' and increase the electron concentration in the SOI layers. Since, in our material the influence of the dislocation network was much stronger—*R* was reduced by 4 orders of magnitude—we believe that this effect is related to enhancement of both, the electron concentration and the electron mobility. This is consistent with the observation of ballistic transport at dislocations in Si.[20]

2.4. Dislocation-Related D band Luminescence

Dislocations are known to cause a quartet of the so-called D lines in the luminescence spectrum of Si,[21] see Figure 9. The origin of the D4 and D3 lines is known. D4 is formed by the transition between the one-dimensional dislocation bands, which are caused by the elastic strain field around the dislocations. The dislocation bands are located about 70–80 meV below the conduction or above the valence band, respectively. The D3 line is a phonon replica of D4. However, the energy levels that form D1 and D2 lines are still under discussion. Recent results suppose that the D1 line is a result of carrier transition between two, relatively deep (0.29 eV) and relatively shallow energy levels (0.09 eV) in the bandgap.[22] These levels correspond well to dislocation-related DLTS peaks. Moreover, the value of the sum 0.29 eV (relatively deep level) + 0.09 eV (shallow level) + 0.8 eV (D1 line) is close to the energy of the Si bandgap.

The intensity of the dislocation luminescence seems to depend on the impurity level. So, it was found that a certain metal contamination was necessary to observe the D1 line luminescence.[23] At higher metal contamination levels the luminescence decreases again. Moreover, oxygen also seems to influence the D1 luminescence.[24] It has to be noted, however, that the impact of impurities on D band luminescence is controversial and still under debate. More details are given in the comprehensive work about D band luminescence.[25]

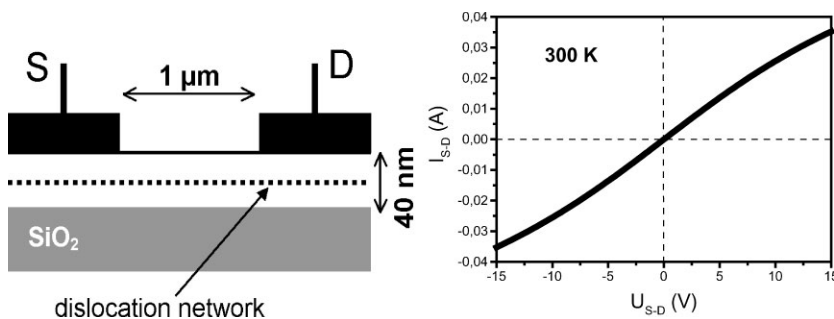

Fig. 8. a) Schematic view of the sample containing a dislocation network within a 40 nm tick SOI layer of p-type conductivity. The Ohmic contacts (S and D) are 5 µm wide and located at a distance of 1 µm. b) I–V characteristics at 300 K revealing Ohmic character, yielding $R_{disl} = 4 \times 10^{2}\,\Omega$. Note, that with decrease of measurement temperature the resistance R_{disl} was reducing. For the reference sample without dislocations $R_{ref} = 2 \times 10^{6}\,\Omega$ was found.

3. Dislocation Networks Produced by Silicon Wafer Direct Bonding

The application of dislocations in devices requires their reproducible formation in defined areas and by applying techniques compatible to CMOS technology. Semiconductor wafer direct bonding using hydrophobic surface conditions is such a method allowing the formation of controlled dislocation networks. In combination with generally applied pattern formation and dry etching processes dislocation networks are also

 © 2009 WILEY-VCH Verlag GmbH & Co. KGaA, Weinheim

produced in defined areas. Furthermore, because dislocation networks in bonded wafers appear only in the interface they may be assumed as two-dimensional structures. This is important if they are implemented into thin SOI architectures.

Because the bonding process assumes that wafers of a finite thickness are involved (which is about 900 μm for wafers having a diameter of 300 mm) additional post-thinning techniques are required to adjust the generated dislocation network in a defined depth below the surface. This can be done either by a combination of mechanical grinding and polishing (CMP) processes, if depths of a few micrometers are necessary, or, if a depth of the dislocations network only of a few nanometers is required, by a combination of wafer bonding and hydrogen-induced layer splitting (Fig. 10). Both methods are described in detail elsewhere.[26]

Semiconductor wafer direct bonding is today's most important technique for fabrication of advanced substrates such as SOI used for high-performance applications. The transfer of a thin silicon layer to an oxidized Si handle wafer assumes hydrophilic surface conditions. If, however, the oxide layers are removed from both wafers, e.g., by dipping in diluted HF solutions, than 2 hydrophobic silicon surfaces are brought into contact. During subsequent annealing dislocations are formed in the interface in consequence of the misorientation between both surfaces. For instance, bonding of Si(100) wafers cause a Σ1 (100) small angle GB characterized by a square-like mesh of screw dislocations expected from theory, see Figure 11.[27] These dislocations are formed by the rotational misfit (twist) between both crystal lattices. There is, however, an additional tilt component caused by the deviation on the [001] axis of real wafers (cut-off). The tilt component is compensated by a periodic array of 60° dislocations. The spacings between dislocations S in both networks are indirectly proportional to the misalignment angle and are given by

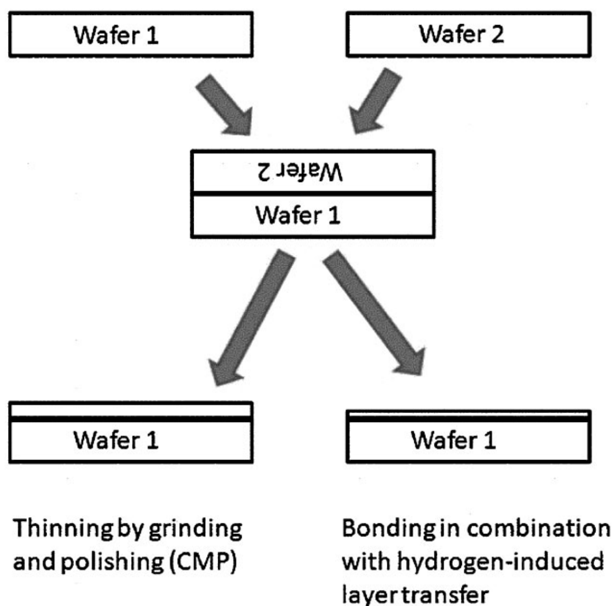

Fig. 10. Schematic presentation of the wafer bonding and post-thinning techniques. Two wafers were bonded using hydrophobic surface conditions. After a subsequent annealing step (not shown in the schema) thinning of one of the wafers is necessary to adjust the dislocation network in a defined depth below the surface. This is performed either by mechanical grinding and polishing techniques (CMP), or by combination of the bonding process with hydrogen-induced layer splitting. The former thinning process is applicable for depths of a few micrometers, while the latter results in depths only of a few nanometers.

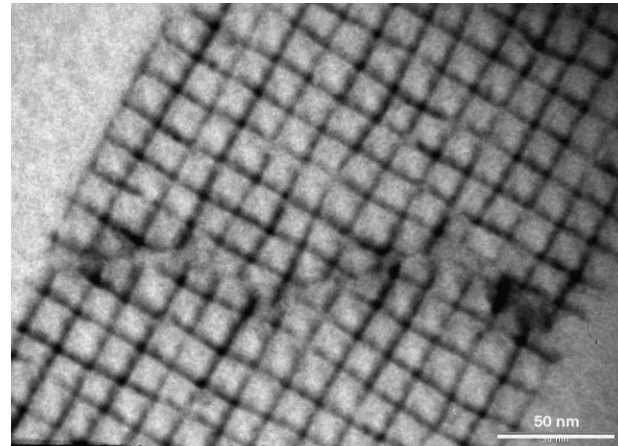

Fig. 11. Plan-view image (25° beveled sample) of the dislocation network in a bonded Si(100)/Si(100) interface. Screw dislocations form a network having square-like meshs and are caused by the twist component. The network is superimposed by a second network of 60° dislocations produced by the tilt component. Measurements of the dislocation spacings result in a tilt angle of 0.12° and a twist angle of 0.63°.

$$S_{\text{twist}} = \frac{a}{2\sqrt{2}\ \sin\frac{\vartheta_{\text{twist}}}{2}}$$

for the screw dislocation network. On the other hand, the relation between dislocation distance and tilt angle of the network formed by 60° dislocations follows as ϑ

$$S_{\text{tilt}} = \frac{a}{\sqrt{2}\ \tan\vartheta_{\text{tilt}}} \infty$$

In both equations a means the lattice constant (which is $a = 0.543$ nm for Si) and ϑ_{twist} and ϑ_{tilt} are the angles of misorientation of the twist and tilt component, respectively.

Variations of the tilt and twist angles are the most important factors effecting the morphology and structure of the resulting dislocation network. Strong modifications of the resulting network are obtained especially at very low twist and tilt angles ($\vartheta_{\text{tilt}} \cong \vartheta_{\text{twist}} < 0.1°$) where the mesh size of the screw dislocation network reaches the same values as the distance of the 60° dislocations. At ($\vartheta_{\text{tilt}} \cong \vartheta_{\text{twist}} \cong 0.07°$) dislocation networks with hexagonal meshes appear in the Σ1 (100) small angle GB. This is caused by the different reaction where a third dislocation is involved. Detailed analyses are discussed elsewhere.[26] Very small twist and tilt angles can be realized experimentally only by aligned wafer bonding allowing the control of the twist angle up to $\vartheta_{\text{twist}} = \pm 0.005°$.[28,29] At $\vartheta_{\text{twist}} \leq 0.001°$ dislocation networks were not observed. Instead, segments of individual dislocations of different geometries were found. Straight segments of screw dislocations are observed first, while—probably at lower angles—loops of various geometries are dominant.[28]

 © 2009 WILEY-VCH Verlag GmbH & Co. KGaA, Weinheim

The electrical and luminescence properties of dislocation networks in the interface of hydrophobic bonded wafer pairs were intensively studied over the last years.[30] EBIC measurements, for instance, proved the recombination activity and contamination level. In samples bonded with an extremely small misorientation angle, e.g., $\sim 0.001^\circ$, the contamination degree of the individual dislocations in the network with metal impurities was estimated as $\sim 10^4\,cm^{-1}$. The temperature dependence of the EBIC contrast gave the energy position of dislocation related states at ~70 meV below the conduction band or above the valance band, in good agreement with DLTS results.[30]

The luminescence properties of dislocation networks are probably most important for future applications as on-chip CMOS-compatible light emitting devices for optical data communication. Figure 12 shows the luminescence spectra of different bonded samples. The spectra are obtained from samples having different misorientation. Detailed photoluminescence and cathodoluminescence measurements provide direct evidence that the wavelength of light emitted from the dislocation network could be tailored to some extent by misorientation of the wafers during bonding procedure. There are three CL spectra in Figure 12 obtained from dislocation networks with various grades of misorientations at 77 K. D1 or D3 lines have the largest intensity in the spectra due to the variation of twist angle from 8.2 to 9°. Thus, the luminescence spectrum can be tailored by the misorientation angles in a controlled manner and the dominance of either D1 or D3 radiation can be attained. Furthermore, in some special cases the D1 emission could completely dominate the spectrum, even at RT.[30] The intensity of the D1 emission is at least ten times larger than that of BB emission at RT. In the panchromatic image of the luminescence from the cross-section of sample with dislocation network the luminescence is distributed only close to the bonded interface and the profile of the signal exhibits a Gaussian-like shape. This inconsistency with the diffusion-like behavior of minority carriers in the

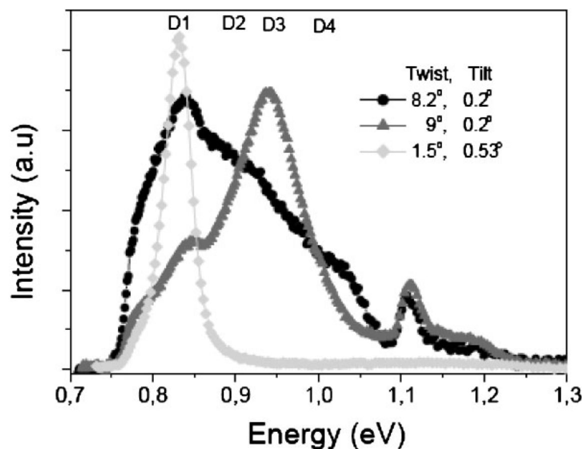

Fig. 12. Impact of the misorientation/dislocation structure on the luminescence spectra of the dislocation networks. The misorientations (tilt and twist components) are indicated in the Figureure.

samples could be attributed to the changes in the distribution of excited minority carriers near the bonded interface due to the electric field generated by the dislocation network.

4. Potential Application of Dislocations for Novel Si Devices

4.1. Light Emitting Diodes Based on Dislocation Networks

Currently used interconnects based on Cu wiring will cause serious problems in the future such as heat penalty, non-acceptable delay and complexity, crosstalk, etc. On-chip optical interconnects are believed to be able to overcome these problems. Several CMOS technology compatible photonic components have already been demonstrated. However, a Si-based light emitter, which is compatible with CMOS technology, is still lacking. We have demonstrated a MOS-LED[31] and a p-n LED—making use of D line radiation described in chapter 2.4—emitting at ~1.5 μm (D1 line) which are based on a dislocation network formed during direct bonding of Si wafers.[32] In another publication,[33] we reported electro-luminescence (EL) around 1.5 μm from dislocation loops formed after Si ion implantation and annealing.

4.1.1. Dislocation-Based MOS-LED

EL with BB emission at about 1.1 μm was reported from a MOS tunnel diode prepared on n-type Si.[34] Under positive gate bias electrons are attracted, building an accumulation layer close to the Si/oxide interface, and a hole current is formed by tunneling through the oxide layer. Also the MOS tunnel diodes on p-type Si yield comparable results. The basic processes in MOS-LEDs are schematically represented in.[31] When a dislocation network with appropriate structure is positioned near the Si/oxide interface the radiative recombination is dominated by the D1 peak at about 1.5 μm instead of the BB peak. This is clearly seen from the EL spectra shown in Figure 13. The MOS-LED on p-type Si, with the dislocation network at a depth of about 45 nm, consisted of a 134 nm thick Ti gate deposited on 1.8 nm thick Si oxide. For further details see.[35] The tunnelling current increases with increasing gate voltage, leading to an enhancement of the EL intensity. Increase in temperature was found to reduce the EL efficiency. Nevertheless, we suppose that sufficient 1.5 μm luminescence at 300 K is achievable with dislocation networks, since clearly detectable D1 emission at 300 K (efficiency > 0.3%) was demonstrated already for a p-n LED containing a dislocation network, see below. Prospects for improvements of the MOS-LED are discussed in.[31]

4.1.2. Dislocation-Based p-n LEDs

Another way to get EL from the dislocation network is injection of excess carriers by a forward biased p-n junction, see Figure 14a. A corresponding EL spectrum measured at RT

 © 2009 WILEY-VCH Verlag GmbH & Co. KGaA, Weinheim

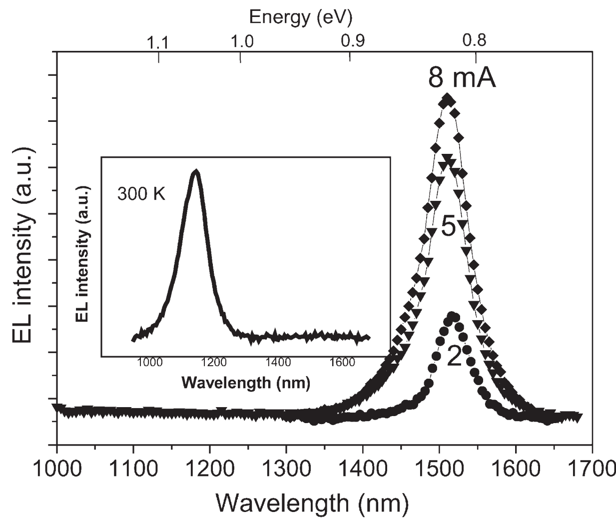

Fig. 13. EL at 80 K of a MOS-LED under gate bias with 1.5 μm radiation caused by the dislocation network. The intensity is found to increase sub-linearly with increasing tunneling current as seen from the spectra measured at 2, 5, and 8 mA. The insert shows at 300 K the reference spectrum of a MOS-LED without network.

is shown in Figure 14b. The dislocation network was located in about 2 μm depth and produced by direct bonding of two p-type (100) Si wafers with 15 Ω cm resistivity. The p-n junction was formed by P doping. The internal efficiency at RT was measured at a forward current of 5 mA. It yields 0.95% for the band–band line and 0.31% for the D1 line. The structure of the LED was mesa-like with an area of the p-n junction and network of ~0.14 mm^2. It is important to note that the excess carriers are transported along the dislocation network (e.g.,[30,36]) which reduces their concentration and decreases the intensity/efficiency of light emission. This effect can be suppressed by using a mesa-like LED structure for carrier confinement. The depth of the dislocation network (distance between p-n junction and network) affects the spectrum and the ratio between D band and BB luminescence. This is shown in the insert of Figure 14b, where the EL spectra of similar dislocation networks located in 2 or 0.26 μm depth, respectively, are compared. Instead of dislocation networks also dislocation loops formed by implantation of Si ions and subsequent anneal can be used as D1 line light emitters,[33] see below.

4.1.3. Stark Effect at Light Emitting Dislocations

Diodes formed by boron diffusion into n-type Si were implanted with Si^+ ions and subsequently annealed to form dislocation loops. The dislocation loops were located close to the p-n junction, i.e., within the junction space charge region. The EL spectrum of the diode appearing under forward bias exhibits the dislocation related D bands where D1 dominates.

The dependence of the spectral position of the D1 line on the *forward* current density was observed in EL. An increase in the forward current corresponds to a reduction of the electric field F in the junction. In Figure 15a the spectral position of the D1 peak is presented as a function of the electric field F, exhibiting a red shift with increase in F. The field was estimated from the junction parameters and the I–V curves. A thermal mechanism of this shift, related to the increased carrier injection, can be excluded because heating should cause a red shift. A *reverse* bias U_R applied to the p-n junction enhances the field F and led to a further growth of the red shift of the D1 peak. For this analysis under reverse bias, the excess carriers were pumped optically. The influence of the bias/electric field on the spectral position of the D1 light is sketched in Figure 15b. The observed red-shift of the D1 peak with increase in the field F can be understood in terms of the Stark effect, e.g.,[37] which implies a quadratic shift in the excitonic transition energy E_{ex} caused by an electric field. The relation $E_{ex} = E_{ex}(0) - \alpha F^2$, where $E_{ex}(0)$ is the energy of excitonic transition at $F = 0$ and α is a characteristic coefficient. Fitting the experimental data presented in Figure 15a yields $E_{ex}(0) = 795$ meV and $\alpha = 0.0186$ meV $(\text{kV cm}^{-1})^{-2}$. The Stark effect on dislocations, which appears to be considerably strong, was observed for the first time; for more details see.[38]

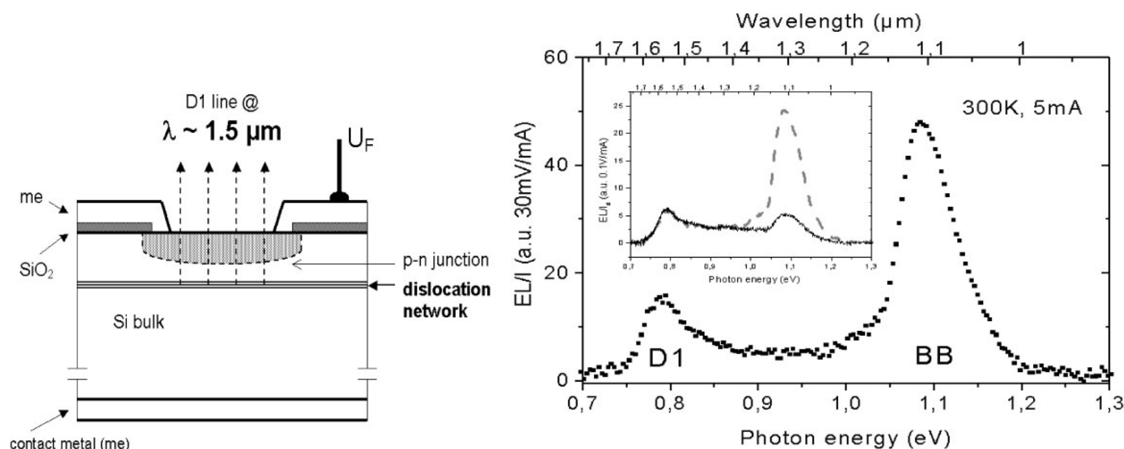

Fig. 14. a, left) Schematic view of a p-n LED based on D1 emission generated by a dislocation network. b, right) EL spectrum at 300 K for a 2 μm deep dislocation network yielding an efficiency >0.3% for the D1 line at 1.55 μm and ~1% for the BB line. The insert shows the influence of the distance between p-n junction and dislocation network: network depth 0.26 μm for the full and 2 μm for the dashed line.

 © 2009 WILEY-VCH Verlag GmbH & Co. KGaA, Weinheim

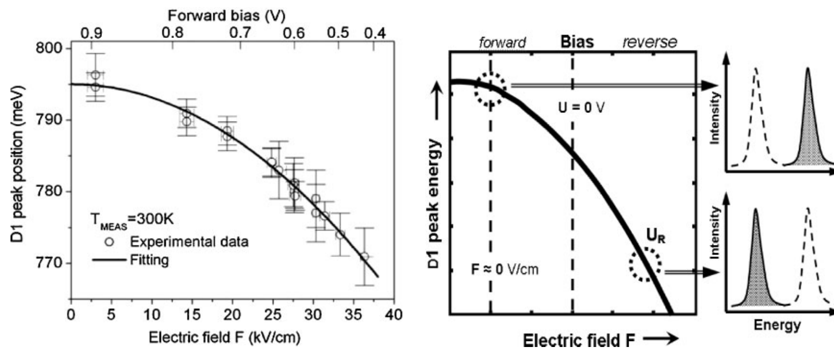

Fig. 15. Influence of electric field on spectral position of the D1 line due to Stark effect. (Left) Dependence of energy position of D1 peak on forward bias at 300 K. The electric field which was calculated from diode parameters and I–V characteristics. The data can be fitted by taking into account the quadratic Stark effect, see.[38] A red-shift of the D1 line is observed when increasing the field/reducing the forward bias. (Right) Schematic illustration of the shift of the spectral position of the D1 line caused by the electric field.

It allows a controlled tuning of the spectral position of the D1 peak. If the spectral shift can be performed in a sufficiently short time, a combination of an electro-optical modulator with the light emitter can be realized. A fast modulation of the field F might be achieved with a reverse rather than with a forward bias.[39]

4.2. Further Intended Applications of Dislocations for Novel Si Devices

4.2.1. Device Concepts Based on the Extraordinary Transport of Charge Carriers Along Dislocations in Si

In Section 2.3 the properties of dislocations in Si were shortly described regarding the extraordinary transport of minority and majority carriers. These effects might be exploited for novel devices.

Minority charge carriers were observed to be transported along the dislocations in Si over a centimeter distance. This effect could be applied for carrier transport as shown in Figure 16a. A forward biased p-n junction close to the dislocation line (network), which runs parallel to the surface, can act as a source of excess minority carriers. For collection of the carriers a reverse-biased p-n junction can be applied, acting as a drain. An important advantage of such dislocation-based channel is that its transport behavior can be controlled/varied in an active manner. A p-n junction between source and drain can be used as an on/off-switch or for modulation of the carrier transport along the channel. Another important feature is the possibility to design a changeover switch/splitter that allows the carriers to (partially) switch from one dislocation line to its next neighbor. For this function a MOS stack in depletion/inversion, crossing the dislocation lines, can be used. Figure 16b shows this for a horizontal switch between two dislocations. The same principle can be applied to switch the carrier transport between dislocations at different depths (vertical gate stack). Hence, a variety of elements are available to fabricate an active 3-D network of dislocation channels.

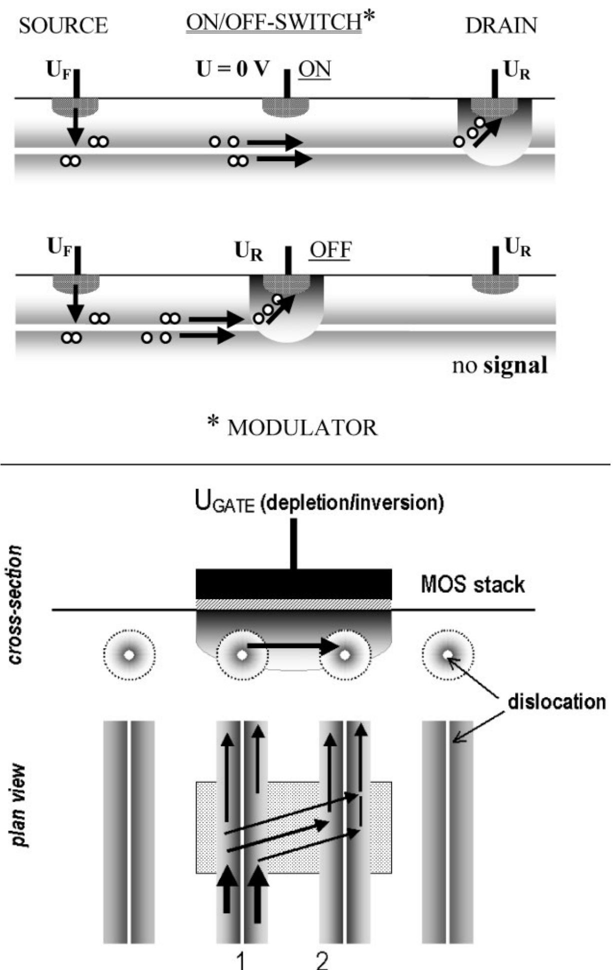

Fig. 16. Example of elements for active control of conduction in dislocation networks (schematically): a, top) on/off switch or modulator, b, bootom) change-over switch/splitter.

The strong enhancement of the transport/mobility of majority charge carriers may be understood in terms of *ballistic transport* at dislocations in Si.[20] Accordingly, an FET containing proper dislocations within its channel may achieve THz performance, due to the expected ballistic transport of the carriers. Figure 17 schematically represents the layout of such a fast device. The channel is formed by a dislocation which is embedded in an SOI nanorod. For simplicity, the gate around the nanorod channel is not shown.

4.2.2. Spatial Control of Biomolecule Immobilization on Si Surfaces

Lateral spatial control of biomolecule immobilization on silicon surfaces is a crucial step for novel biodevices and will allow Si electronics to be combined with biological applications. Coulomb interaction between biomolecules on the top of a Si substrate and the dislocations inside

 © 2009 WILEY-VCH Verlag GmbH & Co. KGaA, Weinheim

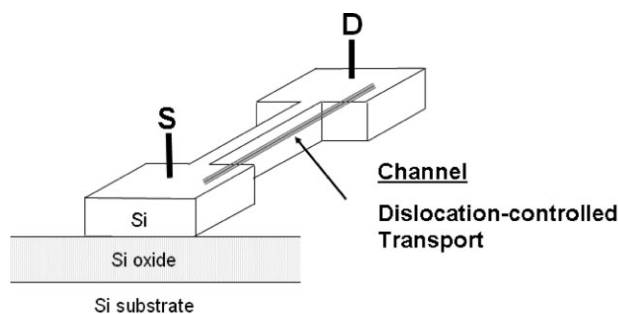

Fig. 17. Schematic layout of a novel FET. The fast/ballistic transport in the channel is controlled by a dislocation embedded in a Si nonorod. The gate around the nanorod is not shown.

the Si substrate is an important concept for such manipulation (Fig. 18a). As desribed above, dislocations in Si are known to form charged lines, which are negatively charged in n-type Si and positively charged in p-type material, respectively. If the dislocations are located close enough to the Si surface an electric strey field is formed above the Si surface that may attract charged biomolecules of opposite charge.[40] The charge state of many biomolecules can be tuned. For example, it depends on the pH-value of the aqueous solution with proteins, e.g.,[41,42] see (Fig. 18b).

Several important parameters of the system can be preset by bonding and treatment procedures in the case of dislocation networks. For example, the dislocation line charge—which has strong influence on the dislocation electric field—can be enhanced by controlled doping of the dislocations with metal atoms and the depth of the dislocation network below the Si surface can be adjusted by well-established layer transfer techniques, etc. All these should allow tailoring the network for the charge, size, and other properties of biomolecules to be manipulated. Moreover, the charge state of various biomolecules could be tuned as well.

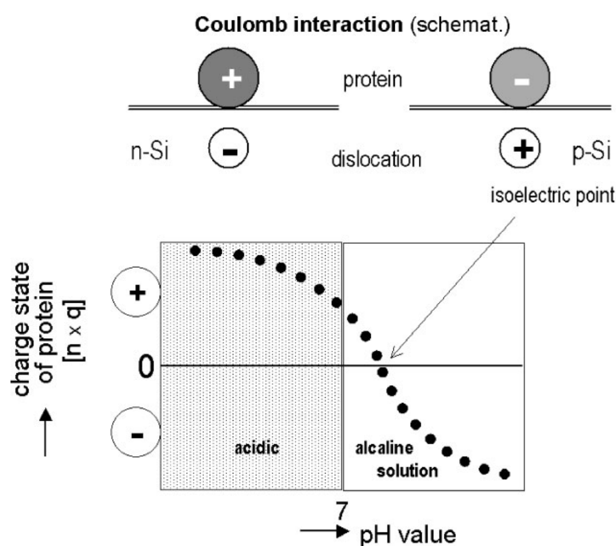

Fig. 18. Coulomb interaction of charged biomolecules with charged dislocation a, top) and dependence of charge state of proteins on pH value of solution b, bottom).

Several steps were already performed in direction of the realization of the concept, see, e.g., ref.[30]

4.2.3. Si-based Thermo-electrical Generators with High ZT

During IC operation electrical energy is transformed into heat leading to a considerable increase in the chip temperature. Recycling of the IC heat dissipation in electrical energy is of great practical interest, for example to increase the serviceable life of mobile systems/phones before recharching of the battery is required. A novel thermo-electric generator making use of Si nanostructures containing dislocation networks might be used for this purpose. The figure of merit of thermo-electric material components is the dimensionless number ZT. Bulk Si has ZT $\sim$ 0.01 only. In detail ZT depends on the electrical resistivity ρ, the thermal conductivity κ, the Seebeck coefficient S and the temperature T of the material: $ZT = S^2T/\rho\kappa$, e.g., ref.[43] As described above (see, e.g., Fig. 8), incorporation of dislocation networks within thin SOI layers reduces the electrical resistivity ρ of Si considerably. Moreover, we also believe that the thermal conductivity κ, will be reduced by the dislocation network due to increased phonon scattering. Such SOI structures containing dislocations are expected to reach ZT values $\gg$0.01. Corresponding electro-optical generators can be monolithically integrated. Moreover, this structure might also be used for a novel Si-based Peltier cooling device.

5. Final Remarks

We have demonstrated several concepts of possible future application of dislocation networks/dislocations fabricated by Si wafer direct bonding. Light emitters with 1.5 μm radiation based on dislocations are demonstrated already, with an efficiency potential estimated at 1% for RT. Experiments are under way to explore the proposed utilization of dislocations in other devices as well. It should be noted, that instead of networks also arrays of parallel dislocations could be formed, e.g., by bonding of (100)/(110) wafers.

Received: August 29, 2008
Final version: December 12, 2008
Published online: March 4, 2009

[1] F. Calzecchi, P. Gondi, F. Schintu, *Nuovo Cimento* **1968**, *58B*, 376.
[2] S. Mil'shtein, V. I. Nikitenko, *Phys. Tech. Semicond.* **1972**, *6*, 1556.
[3] S. Mil'shtein, *J. Phys.* **1979**, *40*, C6.
[4] D. M. Lee, J. B. Posthill, F. Shimura, G. A. Rozgonyi, *Appl. Phys. Lett.* **1988**, *53*, 370.
[5] J. Hornstra, *J. Phys. Chem. Solids* **1958**, *5*, 129.
[6] W. Schröter, H. Cerva, *Solid State Phenomena* **2002**, *85*, 67.
[7] P. R. Wilshaw, G. R. Booker, *Inst. Phys. Conf. Ser.* **1985**, *76*, 73.

[8] M. Kittler, C. Ulhaq-Bouillet, V. Higgs, *J. Appl. Phys.* **1995**, *78*, 4573.
[9] M. Kittler, W. Seifert, *Solid State Phenomena* **2004**, *95*, 197.
[10] H. Blumtritt, M. Kittler, W. Seifert, *Inst. Phys. Conf. Ser.* **1989**, *104*, 233.
[11] S. Pizzini, M. Acciarri, E. Leoni, A. Le Donne, *Phys. Status Solidi B* **2000**, *222*, 141.
[12] V. Higgs, M. Kittler, *Appl. Phys. Lett.* **1994**, *65*, 2804.
[13] O. F. Vyvenko, O. Krüger, M. Kittler, *Appl. Phys. Lett.* **2000**, *76*, 697.
[14] V. Kveder, M. Kittler, W. Schröter, *Phys. Rev. B* **2001**, *63*, 115208.
[15] S. Pandelov, W. Seifert, M. Kittler, J. Reif, *J. Phys.: Condens. Matter* **2002**, *14*, 13161.
[16] O. Krüger, W. Seifert, M. Kittler, O. F. Vyvenko, *Phys. Status Solidi B* **2000**, *222*, 367.
[17] a) M. Kittler, M. Reiche, W. Seifert, X. Yu, T. Arguirov, O. F. Vyvenko, T. Mchedlidze, T. Wilhelm, *ECS Trans.* **2006**, *3*, 429. b) M. Kittler, M. Reiche, T. Arguirov, T. Mchedlidze, W. Seifert, O. F. Vyvenko, T. Wilhelm, X. Yu, *Solid State Phenomena* **2008**, *131*, 289.
[18] T. Mchedlidze, T. Wilhelm, X. Yu, T. Arguirov, G. Jia, M. Reiche, M. Kittler, *Solid State Phenomena* **2008**, *131*, 503.
[19] Y. Ishikawa, K. Yamauchi, C. Yamamoto, M. Tabe, *MRS Proc.* **2005**, *E6.5.1*, 864.
[20] V. Kveder, A. E. Koshelev, T. Mchedlidze, Yu, A. Osip'-yan, A. I. Shalynin, *Sov. Phys. (JETP)* **1989**, *68*, 104.
[21] N. A. Drozdov, A. A. Patrin, V. D. Tkachev, *JETP Lett.* **1976**, *23*, 597.
[22] M. Kittler, T. Arguirov, T. Mchedlidze, M. Reiche, W. Seifert, M. Trushin, T. Wilhelm, X. Yu, in, *Proceedings 5th International Symposium on Advanced Science and Technology of Silicon Materials*, Kona, Hawaii, November 10–14 **2008**, pp. 55–59.
[23] V. Higgs, M. A. Goulding, A. Brinklow, P. Kightley, *Appl. Phys. Lett.* **1992**, *60*, 1369.
[24] T. Arguirov, M. Kittler, W. Seifert, X. Yu, M. Reiche, *Mater. Sci. Eng, B* **2006**, *134*, 109.
[25] V. Kveder, M. Kittler, *Mater. Sci. Forum* **2008**, *590*, 29.
[26] M. Reiche, *Mater. Sci. Forum* **2008**, *590*, 57.
[27] W. Bollmann, *Crystal Defects and Crystalline Interfaces*, Springer Verlag, New York, Heidelberg **1970**.
[28] T. Wilhelm, T. Mchedlidze, X. Yu, T. Arguirov, M. Kittler, M. Reiche, *Solid State Phenomena* **2008**, *131*, 571.
[29] F. Fournel, H. Moriceau, B. Aspar, K. Rousseau, J. Eymery, J.-L. Rouvière, N. Magnea, *Appl. Phys. Lett.* **2002**, *80*, 793.
[30] M. Kittler, X. Yu, T. Mchedlidze, T. Arguirov, O. F. Vyvenko, W. Seifert, M. Reiche, T. Wilhelm, M. Seibt, O. Voß, A. Wolff, W. Fritzsche, *Small* **2007**, *3*, 964.
[31] M. Kittler, M. Reiche, X. Yu, T. Arguirov, O. F. Vyvenko, W. Seifert, T. Mchedlidze, G. Jia, T. Wilhelm, *IEDM Tech. Digest* **2006**, 845.
[32] M. Kittler, M. Reiche, T. Arguirov, W. Seifert, X. Yu, *IEDM Tech. Digest* **2005**, 1027.
[33] T. Hoang, J. Holleman, P. LeMinh, J. Schmitz, T. Mchedlidze, T. Arguirov, M. Kittler, *IEEE Trans. Electron Devices* **2007**, *54*, 1860.
[34] C. W. Liu, M. H. Lee, M.-J. Chen, I. C. Lin, C.-F. Lin, *Appl. Phys. Lett.* **2000**, *76*, 1516.
[35] X. Yu, W. Seifert, O. F. Vyvenko, M. Kittler, T. Wilhelm, M. Reiche, *Appl. Phys. Lett.* **2008**, *93*, 041108.
[36] T. Mchedlidze, T. Wilhelm, X. Yu, T. Arguirov, G. Jia, M. Reiche, M. Kittler, *Solid State Phenomena* **2008**, *131*, 503.
[37] D. A. B. Miller, D. S. Chemla, T. C. Damen, A. C. Gossard, W. Wiegmann, T. H. Wood, C. Burrus, *Phys. Rev. B* **1985**, *32*, 1043.
[38] T. Mchedlidze, T. Arguirov, M. Kittler, T. Hoang, J. Holleman, J. Schmitz, *Appl. Phys. Lett.* **2007**, *91*, 201113.
[39] M. Kittler, M. Reiche, T. Mchedlidze, T. Arguirov, G. Jia, W. Seifert, S. Suckow, I. Willielm, Published by *SPIE*, P. O. Box 10, Bellinglam, Washington 98227-0010 USA **2008**, pp. G1–G7.
[40] M. Kittler, X. Yu, O. F. Vyvenko, M. Birkholz, W. Seifert, M. Reiche, T. Wilhelm, T. Arguirov, A. Wolff, W. Fritzsche, M. Seibt *Mater. Sci. Eng, C* **2006**, *26*, 902.
[41] F. Lottspeich, *Bioanalytik*, Spektrum Akademischer Verlag, Heidelberg, Berlin **1998**, Ch. 10.3.11.
[42] M. Grattarola, G. Massabrio, *Bioelectronics Handbook: MOSFETs, Biosensors and Neurons*, McGraw Hill, New York **1998**.
[43] a) A. I. Boukai, Y. Bunimovich, J. T. Kheli, J. K. Yu, W. A. Goddard, J. R. Heath, *Nature* **2008**, *451*, 168. b) A. I. Hochbaum, R. Chen, R. D. Delgado, W. Liang, E. C. Garnett, M. Najarian, A. Majumdar, P. Young, *Nature* **2008**, *451*, 163.

 © 2009 WILEY-VCH Verlag GmbH & Co. KGaA, Weinheim